Ab initio numerical simulation of left-handed metamaterials: Comparison of calculations and experiments

T. Weiland and R. Schuhmann
Comp. Electromagn. Laboratory, Darmstadt University of Technology, Schossgartenstrasse 8, 64289 Darmstadt, Germany

R. B. Greegor,[a] C. G. Parazzoli, and A. M. Vetter
Physics Technology, The Boeing Company, MS 8H-05, Seattle, Washington 98124

D. R. Smith, D. C. Vier, and S. Schultz
Department of Physics, UCSD, 9500 Gilman Drive, La Jolla, California 92093

(Received 16 February 2001; accepted for publication 20 August 2001)

Using numerical simulation techniques, the transmission and reflection coefficients, or *S* parameters, for left-handed metamaterials are calculated. Metamaterials consist of a lattice of conducting, nonmagnetic elements that can be described by an effective magnetic permeability μ_{eff} and an effective electrical permittivity ε_{eff}, both of which can exhibit values not found in naturally occurring materials. Because the electromagnetic fields in conducting metamaterials can be localized to regions much smaller than the incident wavelength, it can be difficult to perform accurate numerical simulations. The metamaterials simulated here, for example, are based on arrays of split ring resonators (SRRs), which produce enhanced and highly localized electric fields within the gaps of the elements in response to applied time dependent fields. To obtain greater numerical accuracy we utilize the newly developed commercially available code MICROWAVE STUDIO, which is based on the finite integration technique with the perfect boundary approximation. The simulation results are in agreement with published experimental results for the frequencies and bandwidths of the propagation and stop bands associated with the various structures. We further analyze the properties of an individual SRR, and find the dependence of the resonant frequency on the SRR radius, ring thickness, inner/outer radial gap, azimuthal gap, electrical permittivity, and magnetic permeability of the components' materials. Comparison with previously published analytical estimates shows only approximate agreement with the simulation results. [DOI: 10.1063/1.1410881]

I. INTRODUCTION

When describing electromagnetic wave propagation in the presence of a material, it is convenient to describe the response of the material by the material parameters: the electrical permittivity ε and magnetic permeability μ. In a classical material, the material parameters can be directly related to the local charge and current densities. The influence of a material on electromagnetic waves can thus be determined by assigning the local material properties and solving Maxwell's equations for the electromagnetic fields. If the structure is ordered on a macroscopic length scale, the microscopic fields can be averaged over a representative region, resulting in the usual macroscopic fields associated with continuous media. The response of the material can be represented in the effective electrical permittivity ε_{eff} and effective magnetic permeability μ_{eff}.

While this averaging procedure is usually applied to atomic or molecular materials, the process can also be applied to structures composed of macroscopic scattering elements, or electromagnetic metamaterials. Electromagnetic metamaterials are of interest, as the effective material parameters derived for such structures can extend beyond those found in naturally occurring materials. Furthermore, metamaterials may also have additional advantageous physical properties (e.g., thermal, strength, conformability, etc.). A striking example is the recently introduced left-handed metamaterial (LHM), for which the effective magnetic permeability μ_{eff} and effective electric permittivity ε_{eff} were shown to be simultaneously negative over a finite band of frequencies.[1] In this metamaterial, the directions of the macroscopic electric field **E**, the macroscopic magnetic intensity $\mathbf{H}(=\mathbf{B}/\mu_{\text{eff}})$, and the propagation vector **k** associated with a plane wave are related by a left-hand rule, as opposed to the usual right-hand rule obeyed by plane waves in all other known media.[2]

Magnetic effects in naturally occurring materials tend to diminish with increasing frequency. In particular, negative values for the magnetic permeability are very rare, obtainable only in special materials. The left-handed properties, which required both negative permeability as well as negative permittivity, thus could not easily be demonstrated using conventional materials. In the left-handed metamaterial, an array of conducting, nonmagnetic split ring resonators (SRRs) was used to create a region of negative effective

[a]Electronic mail: robert.b.greegor@boeing.com

permeability, while an array of straight conducting posts served as a negative permittivity medium.

There are clear advantages in developing metamaterials with unique or customized effective material parameters; and because conducting elements are such strong scatterers of electromagnetic radiation, metamaterials based on arrangements of conducting elements can exhibit a wide variety of material response. It is thus imperative that accurate numerical techniques be applied that elucidate the electromagnetic properties of both the composite and the fundamental scattering entities as well. Electromagnetic interactions between conducting elements frequently offer particular numerical challenges, as large capacitance between elements can localize the fields to a region much smaller than the wavelength of excitation.

In this work we apply a newly modified approach for the simulation of metamaterials that uses the finite integration technique (FIT) coupled with the perfect boundary approximation (PBA). We apply the approach to both individual SRRs as well as composite media composed of SRRs, and SRRs with wires. We find general agreement between the simulation results and the results of previous measurements on test structures.

II. COMPUTATIONAL APPROACH

Computational methods for reliable field simulations of metamaterials and LHM structures must meet a number of important criteria. Accurate geometric modeling of spatially intricate structures is required. The capacitance between closely spaced conducting elements plays a critical role in the electromagnetic response of metamaterials, as is the case with SRRs. Small errors in describing the geometry corresponding to a highly capacitive region can leverage significant errors in the predicted frequency behavior of the structure.

To obtain accurate predictions for the response of realistic structures, the computational method must be able to model several kinds of materials, including metals with finite conductivity and (possibly dispersive) dielectrics. Losses in metamaterials are a function of both the inherent conductivity of the metals as well as the electromagnetic response of the structure as a whole. In order to predict the effective absorption of a metamaterial via numerical simulation, the computational technique should include the capability of assigning a realistic conductivity to the simulated geometry.

Similar to photonic band gap (PBG) structures, electromagnetic metamaterials can be formed from repeated unit cells containing scattering elements. These periodic structures can be efficiently modeled by simulating the properties of a single unit cell and applying various forms of periodic boundary conditions. While the availability of periodic boundary conditions should therefore be incorporated in any numerical technique, some flexibility must also be granted for structures that deviate from exact periodicity. Defects in otherwise periodic structures, for example, can produce highly localized electromagnetic modes, the detailed patterns of which are often important to consider.

Ultimately, the numerical solution of Maxwell equations produces the local fields. Our goal in analyzing metamaterials is to find macroscopic parameters that average over the local fields associated with the detailed geometry of a structure, thus arriving at a material that can be simply described by effective electrical permittivity ε_{eff} and effective magnetic permeability μ_{eff}. To determine these parameters in a general manner, full access to the field data is needed for postprocessing purposes.

The method used for the studies in this article is the finite integration technique (FIT), which has been successfully used in a wide range of applications in electrical engineering and research during the last few decades.[3] Originally developed independently[4] as a frequency domain approach, it can be regarded as a generalization of the very popular finite difference time domain (FDTD) method.

The FIT is based on a spatial segmentation of the computational domain by a doublet of two computational grids, the primary grid G and the dual grid $\tilde{G}$. The degrees of freedom of the method are so-called integral state variables, which are defined as integrals of the electric and magnetic field vectors over edges L_i and facets A_j of the grid G, or edges $\tilde{L}_j$ and facets $\tilde{A}_i$ of the dual grid, respectively:

$$\begin{aligned} \hat{e}_i &= \int_{\tilde{L}_i} \mathbf{E}\cdot\mathbf{ds} \qquad & \hat{\tilde{d}}_i &= \int_{\tilde{A}_i} \mathbf{D}\cdot\mathbf{dA} \quad \hat{\tilde{j}}_i = \int_{\tilde{A}_i} \mathbf{J}\cdot\mathbf{dA}, \\ \hat{h}_j &= \int_{L_i} \mathbf{H}\cdot\mathbf{ds} \qquad & \hat{\tilde{b}}_j &= \int_{A_j} \mathbf{B}\cdot\mathbf{dA}. \end{aligned} \tag{1}$$

If all these scalar components are collected in algebraic vectors $\hat{\mathbf{e}},\hat{\tilde{\mathbf{d}}},\hat{\tilde{\mathbf{j}}},\hat{\mathbf{h}},\hat{\tilde{\mathbf{b}}}$, Maxwell's equations in their integral form, if evaluated for each facet or cell of the mesh, can be transformed into discrete matrix-vector equations:

$$\begin{aligned} &\oint_{\partial A}\mathbf{E}\cdot\mathbf{ds} = -\frac{d}{dt}\int_A \mathbf{B}\cdot\mathbf{dA} \quad \xrightarrow{\forall A\in\{A_i\}} \quad \mathbf{C}\hat{\mathbf{e}} = -\frac{d}{dt}\hat{\tilde{\mathbf{b}}}, \\ &\oint_{\partial A}\mathbf{H}\cdot\mathbf{ds} = \int_A \left(\frac{\partial}{\partial t}\mathbf{D}+\mathbf{J}\right)\cdot\mathbf{dA} \xrightarrow{\forall A\in\{\tilde{A}_i\}} \tilde{\mathbf{C}}\hat{\mathbf{h}} = \frac{d}{dt}\hat{\tilde{\mathbf{d}}}+\hat{\tilde{\mathbf{j}}}, \\ &\oint_{\partial V}\mathbf{D}\cdot\mathbf{dA} = \int_V \rho dV \xrightarrow{\forall V\in\{\tilde{V}_i\}} \tilde{\mathbf{S}}\hat{\tilde{\mathbf{d}}} = \mathbf{q}, \\ &\oint_{\partial V}\mathbf{B}\cdot\mathbf{dA} = 0 \xrightarrow{\forall V\in\{V_i\}} \mathbf{S}\hat{\tilde{\mathbf{b}}} = \mathbf{0}. \end{aligned} \tag{2}$$

Together with the discrete material relations (for the linear case without permanent polarization)

$$\hat{\tilde{\mathbf{d}}} = \mathbf{M}_\varepsilon\hat{\mathbf{e}}, \quad \hat{\tilde{\mathbf{b}}} = \mathbf{M}_\mu\hat{\mathbf{h}}, \quad \hat{\tilde{\mathbf{j}}} = \mathbf{M}_k\hat{\mathbf{e}}, \tag{3}$$

these so-called Maxwell-grid-equations build a complete system of algebraic equations, which are as general as Maxwell's equations themselves. All matrix operators of the FIT are sparse and (for structured grids) banded matrices, allowing efficient storage and fast computing routines.

The topological matrices **S** and **C**, whose elements can only take the values -1, 1, or 0, fulfill two important properties corresponding directly to the vector analytical properties of the continuous operators:

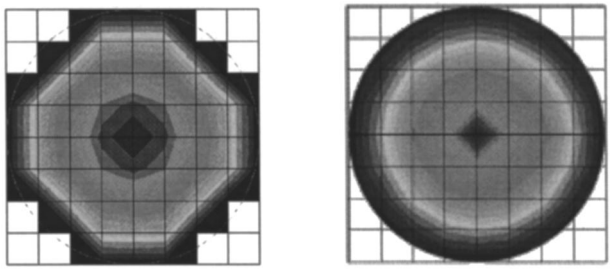

FIG. 1. Electric field strength in a cross section of a spherical cavity. The ''staircase approximation'' using the standard FIT (left) yields strong distortions of the field near curved boundaries, whereas the PBA technique leads to a smooth field distribution. Note that both simulations are based on the same Cartesian grid.

$$\text{div curl} \equiv 0 \leftrightarrow \mathbf{SC} = 0, \quad \tilde{\mathbf{S}}\tilde{\mathbf{C}} = 0,$$
$$\text{curl grad} \equiv 0 \leftrightarrow \mathbf{C}\tilde{\mathbf{S}}^T = 0, \quad \tilde{\mathbf{C}}\mathbf{S}^T = 0. \tag{4}$$

From these relations and the duality property $\tilde{\mathbf{C}} = \mathbf{C}^T$, various consistency and conservation properties of the spatial discretization scheme can be derived, including conservation of charge and energy, orthogonality of eigenmodes, and the stability of time domain schemes.[3] The FIT can therefore be considered as the basis of a unique consistent electromagnetic field theory.

If combined with the leapfrog-time integration scheme, the FIT coincides with the FDTD algorithm[5] and with Pendry's ''Order N-approach'' (ONA),[6] which can be considered as a reformulation of FDTD based on a spectral domain formulation of Maxwell's equations. The resulting explicit algorithm can be considered as a most efficient tool for broadband simulations, as a whole frequency range can be covered by only one transient simulation run. This is a substantial advantage compared to approaches like the boundary element method (BEM) or the finite element method (FEM), as these algorithms have only frequency domain formulations or implicit time stepping schemes. Further, the FIT approach allows a large variety of consistent extensions, including the usage of generalized grids (orthogonal systems like cylindrical or spherical grids, nonorthogonal coordinate-grids, or even consistent subgridding schemes), the modeling of complex material behavior (dispersive, anisotropic, or nonlinear material relations), and the application of advanced time-stepping schemes (implicit schemes, higher-order schemes).

The main disadvantage of the FDTD method (and the ONA), which in its standard form is restricted to Cartesian computational grids, is its poor modeling accuracy for nonorthogonal (oblique or rounded) geometrical objects. For the FIT technique, a number of sophisticated approaches have been developed during the last years to overcome this problem. The most efficient scheme for general applications is the PBA approach,[7] which allows for the use of computationally efficient structured Cartesian grids and simultaneously inhomogeneous material distributions inside single cells. As an example, Fig. 1 shows the electric field strength inside a spherical cavity, calculated with the standard scheme and the advanced PBA technique, respectively. The code MICROWAVE STUDIO (MWS)[8] uses the PBA method and is based on the finite integration technique.

FIG. 2. Array of SRRs plus wire assemblies used for the experiment.

All three-dimensional-grid based methods are limited by computer resources if the computational domain is electrically large (more than 10–20 wavelengths), as the electromagnetic waves must be spatially sampled by a minimum of mesh lines (typically at least ten per wavelength) to obtain accurate results. Thus, for large devices, it is desirable to disassemble the total domain of interest into smaller parts. The simulation process then consists of two steps: the simulation of single components, yielding transfer matrices related to well-defined input and output ports, and the calculation of the overall system behavior by a combination of the single results. A commercial code for this task is CST DESIGN STUDIO (DS).[8] The combination of MWS and DS is the approach taken for the studies presented in this article.

III. COMPARISON OF SIMULATION AND EXPERIMENTAL RESULTS

In the final analysis the validity of the FIT/PBA approach is established by its ability to reproduce experimental results. This will be shown below by a direct comparison between simulations and measurements on various SRR and LHM configurations.[1] We first summarize the experiments.

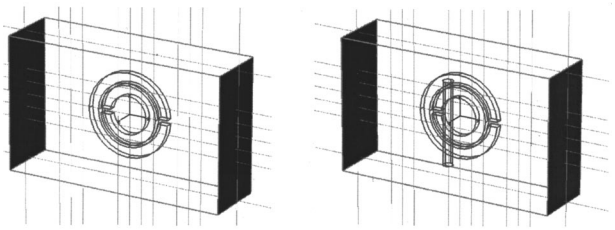

FIG. 3. SRR simulation geometry with and without vertical wire. The SRR and wire dimensions in the simulation and the experiment are $r = 1.5$ mm (inner ring, inner radius), $c = 0.8$ mm (inner and outer ring radial thickness), $d = 0.2$ mm (radial gap between rings), $t = 0.52$ mm (SRR thickness along z), $r_w = 0.4$ mm (wire radius), and $g = 0.4$ mm (azimuthal gap of the rings).

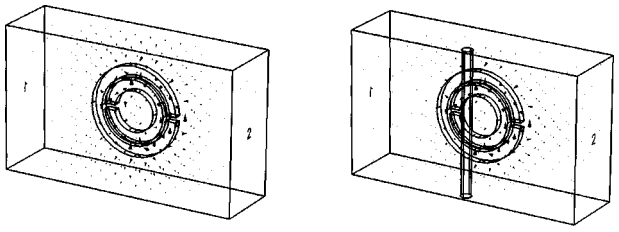

FIG. 4. Arrow plot (logarithmic scale) of the electric field at resonance (4.86 GHz) with and without wire. The scale of the arrow plots is different for the two plots. The effect of the wire was to increase the maximum field strength by a factor of 1.7.

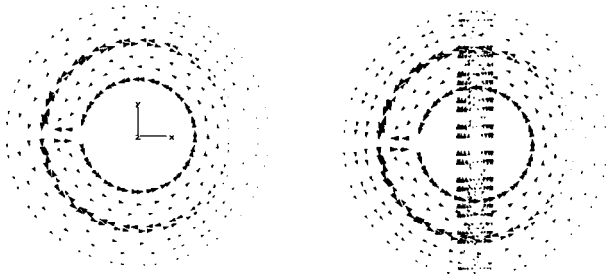

FIG. 5. Arrow plot (logarithmic scale) of the current distribution on the SRR at resonance (4.86 GHz) with and without wire. The scale of the arrow plots is different for the two plots. The effect of the wire was to increase the maximum current by a factor of 1.6.

To experimentally confirm that a single SRR was resonant, a loop antenna was used to couple magnetically to a single SRR (i.e., both loop and SRR axes parallel), with a second loop antenna used to probe the fields on the opposite side. A strong absorption was observed at 4.86 GHz. For a lattice of SRRs the individual resonances are expected to broaden into a band characterized by a negative effective permeability.[9] To simulate an anisotropic infinite array of SRRs, strips of SRRs were cut and placed into a scattering chamber consisting of bounding conducting (aluminum) plates. Because the SRR lattice was placed symmetrically between the plates, and the electric field associated with the exciting radiation was perpendicular to the plates, the metal plates were equivalent to periodic boundary conditions in the vertical direction. The broadened absorption band was indeed measured near 4.86 GHz, consistent with the interpretation of a band of negative effective permeability and positive effective permittivity. The addition of a lattice of vertical posts, as shown in Fig. 2, was expected to generate a frequency region having negative effective electrical permittivity overlapping the region of negative permeability associated with the SRR lattice. The combination of the two media resulted in a propagation band, demonstrated by the reappearance of a transmission region around the 4.86 GHz region.

For the transmission/reflection, or *S*-parameter, calculations, the single SRR and the SRR with a vertical wire were modeled using MICROWAVE STUDIO. The simulated geometries were as shown in Fig. 3.

An automeshing algorithm was used to create the computational grid for the SRR geometry. As the details of the SRR are much smaller than the wavelength, 100 mesh points per wavelength were chosen, resulting in approximately 5000 mesh points for one SRR/wire structure. The excitation pulse had a Gaussian distribution in the time domain that was transformed into 4000 intermediate frequencies from 4–6 GHz in the frequency domain. The ports were at the $\pm x$ limits of the mesh volume where open boundary conditions were used. The structure was excited, as in the experimental case, by a plane wave with the electric field polarized in the y direction and propagating along the x direction. Magnetic boundary conditions were applied at the faces along the axis of the rings ($\pm z$ limits) and electric boundary conditions were used at the $\pm y$ faces of the mesh volume. An $x-z$ symmetry plane was incorporated to reduce the number of mesh points needed, and hence increase the speed of the computation. The rings and the wire were made of perfect electrical conductor (PEC) and were embedded in vacuum surrounded by PEC. The problem was run in time steps satisfying the Courant condition until the residual accuracy was -40 dB, typically taking $\frac{1}{2}$ h or less on an 800 MHz Pentium III processor. The *S* parameters calculated in MWS were passed to DS, where an individual ring or lattice cell could be cascaded into an array of an arbitrary number of cells to calculate the power transmitted through the lattice. The effect of increasing the number of cells in the lattice was to broaden the resonance curve until the array length reached approximately the excitation wavelength. At this point any further increase in the array left the width of the resonance curve unchanged. The run time of DS for array sizes from 8 to 17 rings was on the order of seconds.

The electric field arrow plots at resonance (4.86 GHz) are shown in Fig. 4 with and without wires. The effect of the wire was to increase the maximum field strength.

In Fig. 5 the current distributions in the rings are shown for the SRR at resonance with and without a wire. The largest current flow is concentrated on the surface of the gap

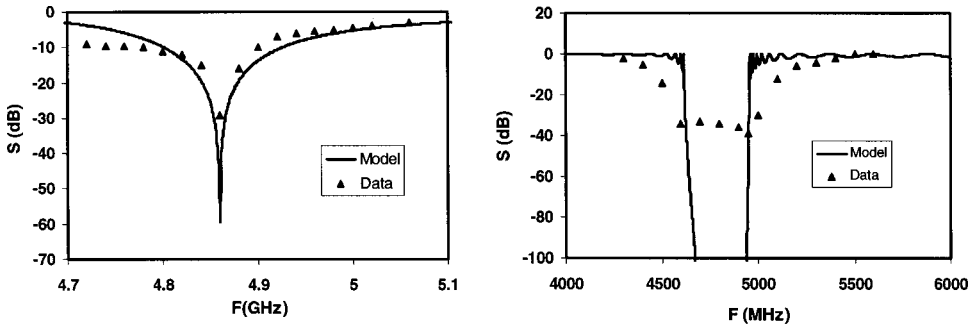

FIG. 6. Simulated and measured absorption of a single SRR (left) and an array of SRRs (right) as functions of frequency.

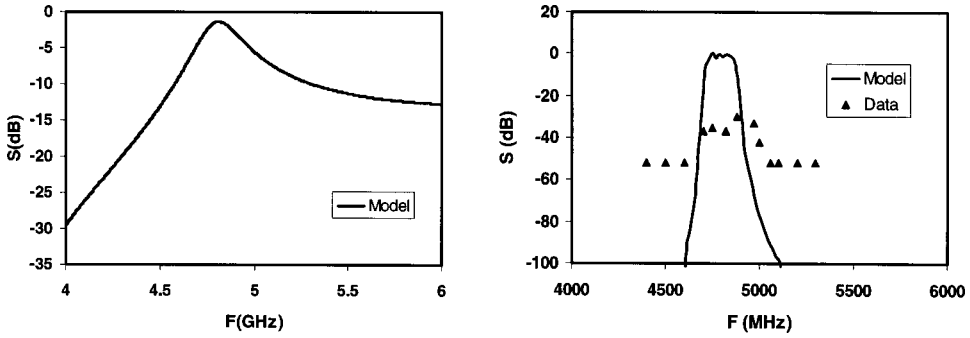

FIG. 7. Simulated and measured absorption of a single SRR plus wire assembly (left) and an array of SRR plus wire assembly (right) as functions of frequency.

between the rings as expected and the current flow has opposite direction in the two rings. The current also is the largest when the wire is present.

In Fig. 6 the comparison between the computed and experimentally measured transmission of a single SRR assembly (without wire) and an array of SRRs (without wires) is shown. The agreement is a good match for the resonant frequency and the general shape of the transmission spectrum. The disagreement between the computed and measured values in the attenuated region can be attributed to the noise level of the instrumentation. In these plots the thickness of the rings was adjusted (within the range of the measured values) to give the best resonance frequency match to the data, to compensate for the rings being suspended in vacuum rather than on circuit board material as in the experiment. As will be shown below, the predominant effect of making small alterations to the resonator geometry is to shift the resonance frequency slightly; thus changing the SRR parameters in the manner described is not expected to produce significant changes in the field patterns or calculated bulk parameters. The calculations for the array of SRRs was performed using the *S*-parameter method as described above.

Figure 7 shows the transmission of a single ring plus wire assembly as a function of the frequency. As expected, the addition of the vertical wire to the SRR changes the behavior from a stop to a bandpass filter. Also shown is the computed and measured transmission of an array of SRRs plus wire assemblies. The observed increase in transmission is smaller than the computed one. The discrepancy may be attributed to the perfect conductivity of the SRRs in the simulation, misalignment of the ring resonators and wires, and to subtle unresolved experimental uncertainties.[10] Although the simulation and experimental data agree reasonably well in this area, more work is needed to understand the discrepancy.

IV. TUNABILITY OF ELECTROMAGNETIC METAMATERIALS

An analytical approximation[9] for the effective permeability of a SRR as a function of the frequency is

$$\mu_{\mathrm{eff}}^{\mathrm{SRR}}(\omega)=1-\frac{\pi r^2}{a^2\left(1-\dfrac{3d}{\varepsilon_0\mu_0\omega^2\pi^2r^3}+\dfrac{2i\sigma}{\mu_0\omega r}\right)}. \tag{5}$$

Here r is the inner ring radius, d is the radial gap between the rings, a is the lattice constant (separation distance between the centers of the rings), and σ is the resistance of the ring material.

The plot of $\mu_{\mathrm{eff}}^{\mathrm{SRR}}(f)$ from Eq. (5), as a function of the frequency in GHz, is given in Fig. 8. The resonant frequency, at which the effective magnetic permeability becomes negative and the left-handed behavior becomes evident, is around 6.4 GHz for the SRR. The explicit expression for the resonant frequency for the SRR is[9]

$$f_{\mathrm{res}}^{\mathrm{SRR}}=\frac{\sqrt{\dfrac{3d}{\mu_0\varepsilon_0\pi^2r^3}}}{2\pi 10^9}(\mathrm{GHz}). \tag{6}$$

The MWS simulation and the experiment predict the resonant frequency for the SRR at 4.86 (GHz). In view of the assumptions used in Eq. (5), the agreement is sufficient to make this formula useful for parametric studies.

The tunability of the structure (i.e., shifting of the resonant frequency) can be achieved in two ways, by changing the characteristic dimension of the SRR or by using materials with adjustable electrical permittivity ε and magnetic permeability μ. From Eq. (6) the resonant frequency scales as $d^{0.5}r^{-1.5}$. We have tested this scaling law in our simulation for the SRR structure with the same geometry as described above. The results are shown in Fig. 9.

From these results we find that the resonant frequency predicted by the simulation scales as $d^{0.21}r^{-0.90}$ rather than $d^{0.5}r^{-1.5}$ as expected from Eq. (6) shown above. As indicated

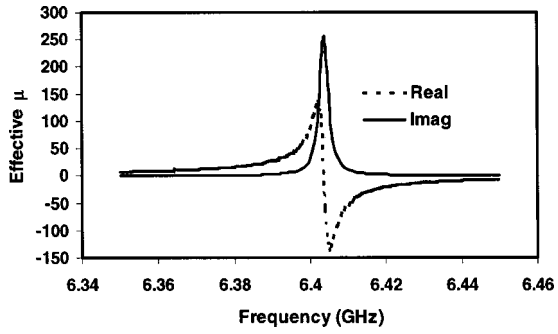

FIG. 8. Effective permeability $\mu_{\mathrm{eff}}^{\mathrm{SRR}}(f)$ for $r=0.15$ cm, $a=0.8$ cm, $d=0.2$ cm, and $\rho=0.0155\ \Omega$ m.

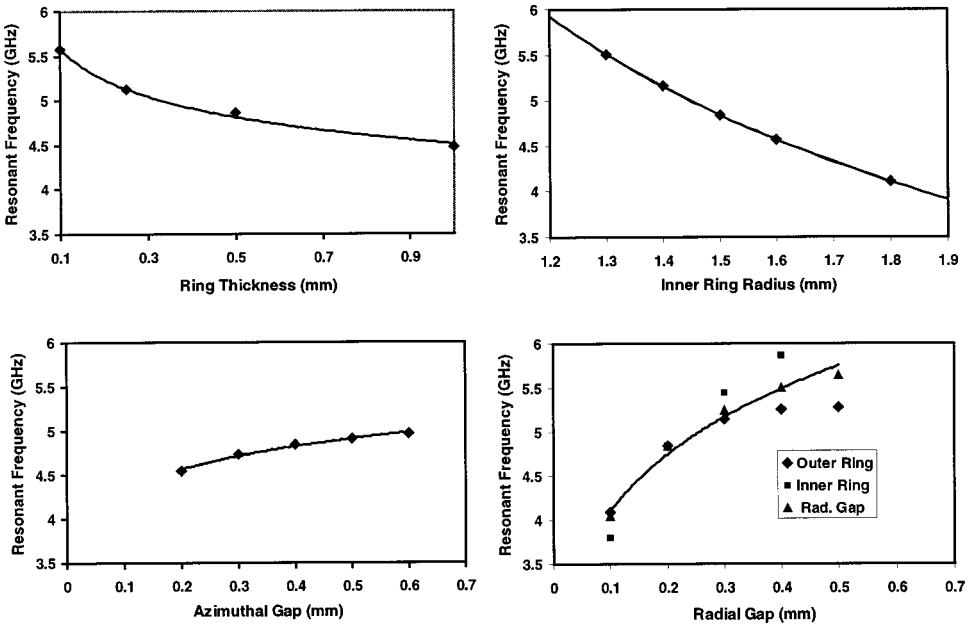

FIG. 9. Effect of geometrical dimensions on the resonant frequency of a single SRR without a wire, from MWS simulations.

in Fig. 9 the simulation also predicts a weak dependence of the resonant frequency on the azimuthal gap ($g^{0.08}$) and thickness ($t^{-0.09}$) of the rings.

Finally the resonance frequency can be tuned by changing the values of ε and μ of the material in which the SRR are imbedded. We have done this in our simulation as shown in Fig. 10, where the dependence of the resonance frequency as a function of ε and μ is shown ($\varepsilon^{-0.52}, \mu^{-0.52}$). We find that $1/f\partial f/\partial\varepsilon \approx -(1/2\varepsilon)$ and $1/f\partial f/\partial\mu \approx -(1/2\mu)$; therefore a factor of 2 increase in ε or μ corresponds to a downward frequency shift of half an octave.

In summary, a limited degree of tunability is possible by changing the ring thickness, radial gap, and/or the inner radius of the rings. Stronger tunability is achieved by controlling the permittivity and permeability of the medium in which the SRRs are embedded.

V. CONCLUSION

In summary we have used the finite integration technique and perfect boundary approximation incorporated in the software codes MWS and DS developed by CST to simulate the response of SRRs, including configurations exhibiting left-handed material properties. For single SRRs the resonance frequency was computed at the experimental value of 4.86 GHz with realistic SRR element dimensions, and the bandpass characteristics were reversed when a wire was included with the SRR. The effect of assembling an array of SRRs was to broaden the stop/bandpass filter characteristics of a single SRR. These results are in good qualitative agreement with experimental measurements. Comparison of the simulations with published analytical estimates of the resonant frequency dependence on various parameters showed only approximate agreement. This was not unexpected in view of the rough assumptions made in the analytical treatment. This study demonstrates that current numerical techniques can be reliably used to predict the response of electromagnetic metamaterials based on conducting elements.

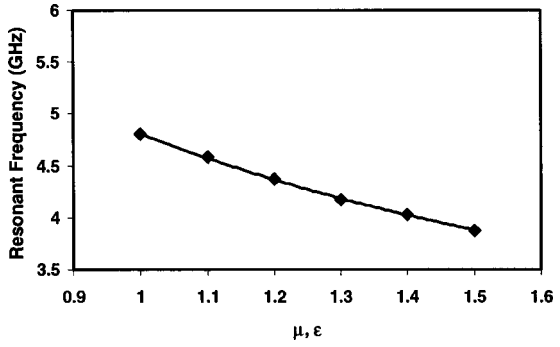

FIG. 10. Resonant frequency of SRR (without wire) as a function of permittivity or permeability.

ACKNOWLEDGMENTS

The authors express our thanks to R. Wong of the Boeing Phantom Works Engineering Computing organization for partial support of this effort, and to CST for providing beta versions of MWS and DS which allowed the simulations to be performed.

[1] D. R. Smith, W. Padilla, D. C. Vier, S. C. Nemat-Nasser, and S. Schultz, Phys. Rev. Lett. **84**, 4184 (2000).
[2] V. G. Veselago, Sov. Phys. Usp. **10**, 509 (1968).
[3] T. Weiland, Int. J. Numer. Modelling: Electron. Networks, Devices Fields **9**, 259 (1996).
[4] T. Weiland, Arch. Elektr. Uebertrag. **31**, 116 (1977).
[5] K. S. Yee, IEEE Trans. Antennas Propag. **14**, 302 (1966).
[6] J. B. Pendry, J. Phys.: Condens. Matter **8**, 1085 (1996).
[7] B. Krietenstein, R. Schuhmann, P. Thoma, and T. Weiland, Nineteeth International Linear Accelerator Conference (LINAC98), Chicago, IL, 1998.
[8] MICROWAVE STUDIO and DESIGN STUDIO are registered trademarks of CST GmbH, Darmstadt, Germany.
[9] J. B. Pendry, A. J. Holden, D. J. Robbins, and W. J. Steward, IEEE Trans. Microwave Theory Tech. **47**, 2075 (1999).
[10] D. C. Vier (private communication).